



## Laminar heat transfer in a moving porous bed reactor simulated with a macroscopic two-energy equation model

Ana C. Pivem, Marcelo J.S. de Lemos\*

Departamento de Energia – IEME, Instituto Tecnológico de Aeronáutica – ITA, 12228-900 São José dos Campos, SP, Brazil

### ARTICLE INFO

#### Article history:

Received 13 January 2011

Received in revised form 14 November 2011

Accepted 14 November 2011

Available online 20 December 2011

#### Keywords:

Moving bed  
Porous media  
Heat transfer

### ABSTRACT

This work investigates the influence of physical properties on heat transfer between the solid and fluid phases in a porous reactor, in which both the permeable bed and the working fluid move in the same direction with respect to fixed bounding walls. For simulating laminar flow and heat transfer, a two-energy equation model is applied in addition to a mechanical model. Transport equations are discretized using the control-volume method and the system of algebraic equations is relaxed via the SIMPLE algorithm. The effects of Reynolds number, solid-to-fluid velocity ratio, permeability, porosity, ratio of solid-to-fluid thermal capacity and ratio of solid-to-fluid thermal conductivity on flow and heat transport are analyzed. The laminar model is validated by means of an analytical solution. Results for concurrent laminar flow indicate that, when the speed of the solid approaches that of the fluid, the strong axial convection of the solid, as well as the reduction of the relative velocity, cause an increase in the axial length needed for thermal equilibrium between phases to occur. Longer thermal developing lengths are also found for higher permeabilities and higher porosities. For higher solid-to-fluid thermal capacities and higher solid-to-fluid thermal conductivity ratios, the temperature of the solid phase shows less axial variation regardless of its velocity in relation to the fluid phase.

© 2011 Elsevier Ltd. All rights reserved.

### 1. Introduction

There is an increasing interest in the use of moving bed technology for chemical compound separation, recuperation of petrochemical processes, drying of grains and seeds and removal of organic matter in effluents, to mention a few applications. The advantages of using a moving bed configuration are low investment, low energy consumption, low maintenance and improvement process performance. Accordingly, granular moving bed configurations are present in a number of engineering systems, including those involving iron ore preparation for steel production, for manufacturing of advanced materials and, more recently, for biomass use in environment-friendly energy production equipment. Before proceeding, one should mention that although most applications in industry are concerned with turbulent flow through permeable beds, here only the laminar flow regime is investigated. By that, one can establish a consistent line of study in order to analyze turbulent flows with appropriate models in the future.

With respect to pelletization of iron ore, Parisi and Laborde [1] and Negri et al. [2] presented a study about the direct reduction of iron oxide in a countercurrent reactor in a moving bed. Also within this context, Valipour et al. [3] developed a mathematical model to

simulate grain kinetics and thermal behavior of a pellet of porous iron oxide. Their study considered chemical reactions with a mixture of hydrogen, carbon monoxide, carbon dioxide and water vapor. Further, Valipour and Saboohi [4] presented a mathematical model to simulate the multiple heterogeneous reactions in a moving bed of porous pellets on a reactor. Valipour and Saboohi [5] described a model to predict flow in a cylindrical reactor in which pellets of iron ore went through a gas mixture.

Henda and Falcioni [6] described the thermal performance of a pre-heater that consists of a moving bed of pellets of nickel in concurrent flow with a gas, using both one and two equations energy models.

Further, biomass pelletization and preparation for energy production may be considered as a system having a moving porous bed. Examples are given by Ryu et al. [7], Boman et al. [8] and Shimizu et al. [9], who presented mathematical models of the gasification a system using a moving bed in the burning of biomass. Already Kayal and Chakravarty [10], Rogel and Aguilón [11] and Nussbaumer [12] investigated technologies to cope with the problem of pollutant emission during of combustion and co-combustion of biomass. Other basic studies on reactive flow in fluidized beds can be found in the literature [13–15].

For thermal analysis of non-reacting systems, Nakayama et al. [16] presented the exact solution of different energy equations, for solid and fluid phases, for cases of engineering interest. They

\* Corresponding author. Tel.: +55 1239475860; fax: +55 1239475842.  
E-mail address: [delemos@ita.br](mailto:delemos@ita.br) (M.J.S. de Lemos).

**Nomenclature**

$A_i$	interfacial area (m <sup>2</sup> )	$Re_D$	Reynolds number based on $\mathbf{u}_{rel}$
$a_i$	interfacial area per unit volume, $a_i = A_i/\Delta V$ (m <sup>-1</sup> )	$\langle T_f \rangle$	fluid temperature (K)
$c_F$	Forchheimer coefficient	$\langle T_s \rangle$	solid temperature (K)
$c_p$	specific heat (J/kg K)	$\mathbf{u}$	microscopic velocity vector (m/s)
$D$	particle diameter, size of square rod (m)	$\langle \mathbf{u} \rangle^i$	Intrinsic (fluid) average of $\mathbf{u}$ (m/s)
$\mathbf{D}$	deformation rate tensor, $\mathbf{D} = [\nabla \mathbf{u} + (\nabla \mathbf{u})^T]/2$ (s <sup>-1</sup> )	$\mathbf{u}_D$	Darcy velocity vector, $\mathbf{u}_D = \phi \langle \mathbf{u} \rangle^i$ (m/s)
$G$	tortuosity parameter	$\mathbf{u}_{rel}$	relative velocity based on total volume, $\mathbf{u}_{rel} = \mathbf{u}_D - \mathbf{u}_s$ (m/s)
$H$	distance between channel walls (m)	$X$	dimensionless coordinate
$h_i$	Interfacial heat transfer coefficient (W/m <sup>2</sup> K)		
$K$	permeability (m <sup>2</sup> )		
$K_{xx}$	axial component of thermal dispersion tensor (W/mK)	<i>Greek symbols</i>	
$k_{stg}$	effective stagnant thermal conductivity of saturated porous medium (W/mK)	$\alpha$	parameter in Eqs. (28) and (29) (negative real root)
$k_s/k_f$	thermal conductivity ratio of solid to fluid	$\gamma$	phase identifier
$L$	channel length (m)	$\mu$	fluid dynamic viscosity (kg/ms)
$p$	thermodynamic pressure (N/m <sup>2</sup> )	$\rho$	density (kg/m <sup>3</sup> )
$\langle p \rangle^i$	intrinsic (fluid) average of pressure $p$ (N/m <sup>2</sup> )	$\phi$	porosity
$Pe$	Peclet number, Eq. (30)	<i>Subscript</i>	
$Pe_d$	Peclet number based on the $D$ and $\mathbf{u}_D$	$s, f$	$s = \text{solid}, f = \text{fluid}$
$Re$	Reynolds number based on $\mathbf{u}_D$		

included in their study heat transfer analyses for one-dimensional porous plate with internal heat generation and thermally developing unidirectional flow through a semi-infinite porous medium. Such two-energy equation model has been investigated by a number of authors and is based on the idea that under certain conditions the two phases, namely the solid and the fluid, cannot have their temperatures considered to be equal and, as such, they need be evaluated using distinct transport equations [17–19].

Accordingly, in a series of papers a macroscopic model for fixed porous media, considering local thermal equilibrium (LTE) between the fluid and solid matrix, was first proposed and applied to non-buoyant [20] as well as to buoyant flows [21]. Later, in order to tackle problems subjected to thermal non-equilibrium, studies on the interfacial heat transfer coefficient between phases were conducted [22,23]. Subsequently, macroscopic laminar flow through a porous reactor was simulated using correlations for interstitial heat transfer [24]. None of the papers just mentioned, however, considered movement of the solid phase. For cases when the solid phase also moves, computations for a moving porous bed were first presented in Ref. [25], which made use of a full macroscopic two-energy equation model [26].

The purpose of this contribution is to extend the work of [25] in order to analyze now the influence of flow parameters and physical properties, of both the solid and the fluid phases, in order to evaluate their impact on temperature distribution and heat transfer in a permeable medium.

### 1.1. Macroscopic model for flow equations

The equations to follow are available in the open literature and for that their derivation are not repeated here [27]. The geometry considered in this work is schematically shown in Fig. 1a. A moving permeable bed with constant velocity travels along the reactor depicted in the figure. Incoming fluid and solid phase have different temperatures at inlet.

### 1.2. Fixed bed

A macroscopic form of the governing equations is obtained by taking the volumetric average of the entire equation set. In this development, the porous medium is considered to be rigid, fixed

and saturated by the incompressible fluid. As mentioned, derivation of this equation set is already available in the literature [27] so that details need not to be repeated here. Nevertheless, for the sake of completeness, the final laminar incompressible form of the equations is here presented:

Continuity:

$$\nabla \cdot \mathbf{u}_D = 0 \quad (1)$$

Momentum:

$$\rho \left[ \frac{\partial \mathbf{u}_D}{\partial t} + \nabla \cdot \left( \frac{\mathbf{u}_D \mathbf{u}_D}{\phi} \right) \right] = -\nabla \cdot (\phi \langle \bar{p} \rangle^i) + \mu \nabla^2 \mathbf{u}_D - \left[ \frac{\mu \phi}{K} \mathbf{u}_D + \frac{c_F \phi \rho |\mathbf{u}_D| \mathbf{u}_D}{\sqrt{K}} \right], \quad (2)$$

where the last two terms in Eq. (2) represent the Darcy and Forchheimer contributions.

### 1.3. Moving bed

For a moving bed, only cases where the solid phase velocity is kept constant will be considered here, or say, we consider here a moving bed that crosses a fixed control volume in addition to a flowing fluid, which is not necessarily moving with a velocity aligned with the solid phase velocity. The steps below show first some basic definitions prior to presenting a proposal for a set of transport equations for analyzing such systems.

A general form for a volume-average of any property  $\varphi$ , distributed within a phase  $\gamma$  that occupy volume  $\Delta V_\gamma$ , can be written as [28,29],

$$\langle \varphi \rangle^\gamma = \frac{1}{\Delta V_\gamma} \int_{\Delta V_\gamma} \varphi dV_\gamma \quad (3)$$

In the general case, the volume ratio occupied by phase  $\gamma$  will be  $\phi^\gamma = \Delta V_\gamma / \Delta V$ .

If there are two phases, a solid  $\gamma = s$  and a fluid phase  $\gamma = f$ , volume average can be established on both regions. Also,

$$\phi^s = \Delta V_s / \Delta V = 1 - \Delta V_f / \Delta V = 1 - \phi^f \quad (4)$$

and for simplicity of notation one can drop the superscript “f” to get

$$\phi^s = 1 - \phi \quad (5)$$

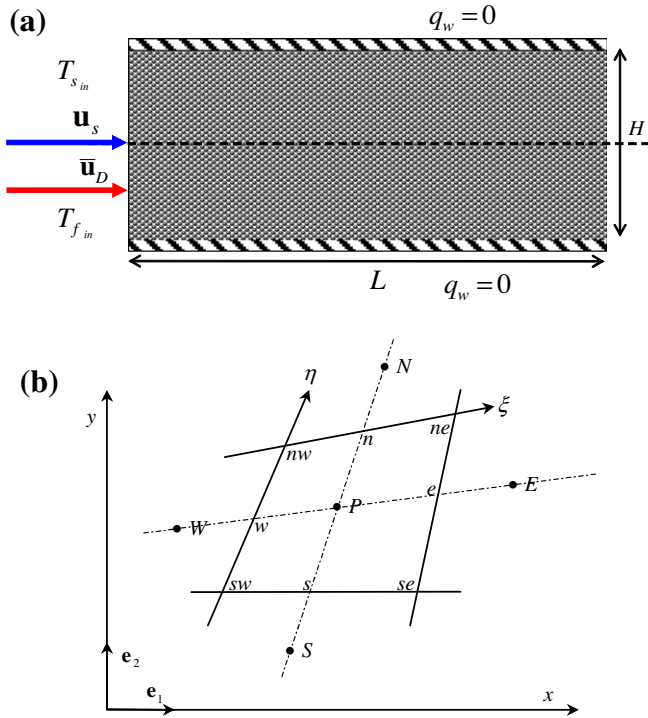


Fig. 1. Physical and numerical models: (a) Porous bed reactor with a moving solid matrix. (b) Control volume and notation.

As such, calling the instantaneous local velocities for the solid and fluid phases,  $\mathbf{u}_s$  and  $\mathbf{u}$ , respectively, one can obtain the average for the solid velocity, within the solid phase, as follows,

$$\langle \mathbf{u} \rangle^s = \frac{1}{\Delta V_s} \int_{\Delta V_s} \mathbf{u}_s dV_s \quad (6)$$

with, in turn, can be related to an average velocity referent to the entire REV as,

$$\mathbf{u}_s = \frac{(1-\phi)}{\Delta V} \frac{1}{\Delta V_s} \int_{\Delta V_s} \mathbf{u}_s dV_s \quad (7)$$

A further approximation herein is that the porous bed is kept rigid and moves with a steady average velocity  $\mathbf{u}_s$ .

Both velocities can then be written as,

$$\mathbf{u}_D = \phi \langle \mathbf{u} \rangle^i \text{ and } \mathbf{u}_s = (1-\phi) \langle \mathbf{u} \rangle^s = \text{const} \quad (8)$$

A relative velocity is then defined as,

$$\mathbf{u}_{\text{rel}} = \mathbf{u}_D - \mathbf{u}_s \quad (9)$$

Assuming that the relative movement between the two phases is macroscopically described by Eq. (9), the momentum equation reads,

$$\rho \left[ \frac{\partial \mathbf{u}_D}{\partial t} + \nabla \cdot \left( \frac{\mathbf{u}_D \mathbf{u}_D}{\phi} \right) \right] = -\nabla \cdot (\phi \bar{p})^i + \mu \nabla^2 \mathbf{u}_D - \underbrace{\left[ \frac{\mu \phi}{K} \mathbf{u}_{\text{rel}} + \frac{C_F \phi \rho |\mathbf{u}_{\text{rel}}| \mathbf{u}_{\text{rel}}}{\sqrt{K}} \right]}_{\text{relative drag}}, \quad (10)$$

#### 1.4. Two-energy equation model

As for the flow, the macroscopic equations to heat transport in porous media are obtained by applying the average volume to

microscopic equations. The mathematical model used to describe the heat transfer between the solid and fluid in a unit of moving bed is based on the two-energy equations model, which can be written as:

$$\begin{aligned} & \{(\rho c_p)_f \phi\} \frac{\partial \langle T_f \rangle^i}{\partial t} + (\rho c_p)_f \nabla \cdot (\mathbf{u}_D \langle T_f \rangle^i) \\ & = \nabla \cdot \{ \mathbf{K}_{\text{eff},f} \cdot \nabla \langle T_f \rangle^i \} + h_i a_i (\langle T_s \rangle^i - \langle T_f \rangle^i) \end{aligned} \quad (11)$$

$$\begin{aligned} & \{(1-\phi)(\rho c_p)_s\} \frac{\partial \langle T_s \rangle^i}{\partial t} + (\rho c_p)_s \nabla \cdot (\mathbf{u}_s \langle T_s \rangle^i) \\ & = \nabla \cdot \{ \mathbf{K}_{\text{eff},s} \cdot \nabla \langle T_s \rangle^i \} - h_i a_i (\langle T_s \rangle^i - \langle T_f \rangle^i) \end{aligned} \quad (12)$$

where,  $\mathbf{K}_{\text{eff},f}$  and  $\mathbf{K}_{\text{eff},s}$  are the effective conductivity tensors for fluid and solid, respectively, given by:

$$\mathbf{K}_{\text{eff},f} = [\phi k_f] \mathbf{I} + \mathbf{K}_{f,s} + \mathbf{K}_{\text{disp}} \quad (13)$$

$$\mathbf{K}_{\text{eff},s} = [(1-\phi)k_s] \mathbf{I} + \mathbf{K}_{s,f} \quad (14)$$

where  $\mathbf{I}$  is the unit tensor and  $\mathbf{K}_{\text{disp}}$ ,  $\mathbf{K}_{f,s}$  and  $\mathbf{K}_{s,f}$  are coefficients defined as,

$$\text{Thermal dispersion : } -(\rho c_p)_f (\phi \langle \mathbf{u}^i T_f \rangle^i) = \mathbf{K}_{\text{disp}} \cdot \nabla \langle T_f \rangle^i \quad (15)$$

$$\text{Local conduction : } \begin{cases} \nabla \cdot \left[ \frac{1}{\Delta V} \int_{A_i} \mathbf{n}_i k_f T_f dA \right] = \mathbf{K}_{f,s} \cdot \nabla \langle T_s \rangle^i \\ -\nabla \cdot \left[ \frac{1}{\Delta V} \int_{A_i} \mathbf{n}_i k_s T_s dA \right] = \mathbf{K}_{s,f} \cdot \nabla \langle T_f \rangle^i \end{cases} \quad (16)$$

where  $\mathbf{n}_i$  in (16) as already noted, is the unit vector pointing outwards of the fluid phase. In this work, for simplicity, one assumes that the overall thermal resistance between the two phases is controlled by the interfacial film coefficient, which considers the boundary layer at the solid–fluid interface, rather than by the thermal resistance within the solid and the fluid phases. Such an assumption might be more valid for turbulent flows, but here it is also employed for laminar cases in the absence of better information. As such, the local conduction coefficients  $\mathbf{K}_{f,s}$ ,  $\mathbf{K}_{s,f}$  are here neglected for the sake of simplicity. Additional information on the models in Eqs. (13), (14) can be found in Ref. [20].

Non-dimensional temperatures for the solid and fluid are defined as:

$$\theta_{s,f} = \frac{\langle T_{s,f} \rangle^i - T_{\text{min}}}{T_{\text{max}} - T_{\text{min}}} \quad (17)$$

where the subscripts  $s, f$  stands for the solid and fluid phases, respectively, and “max” and “min” refers to both temperature maximum and minimum of either phase.

#### 1.5. Interfacial heat transfer coefficient

The heat transferred between the two phases was modeled by means of a film coefficient  $h_i$ , or interstitial heat transfer coefficient, present in Eqs. (11) and (12), such that,

$$\begin{aligned} h_i a_i (\langle T_s \rangle^i - \langle T_f \rangle^i) & = \frac{1}{\Delta V} \int_{A_i} \mathbf{n}_i \cdot k_f \nabla T_f dA \\ & = \frac{1}{\Delta V} \int_{A_i} \mathbf{n}_i \cdot k_s \nabla T_s dA \end{aligned} \quad (18)$$

where  $A_i$  is the interfacial area between the two phases and  $a_i$  is the interfacial area per unit volume or  $a_i = A_i / \Delta V$ . The high values of  $a_i$  make them attractive for transferring thermal energy via conduction through the solid followed by convection to a fluid stream.

Wakao et al. [30] obtained a heuristic correlation for a closely packed bed of particle diameter  $D$  and compared their results with

**Table 1**  
Properties and non-dimensional parameters considered in the investigation.

$\alpha$	$\frac{k_s}{k_f}$	$\phi$	$G$	$k_{eff}/k_f$	$K_{xx}/k_f$
0.625	40	0.4	-0.013219	4.29293	50

experimental data. This correlation for the interfacial heat transfer coefficient is given by,

$$\frac{h_i D}{k_f} = 2 + 1.1 Re_D^{0.6} Pr^{1/3}, \text{ for } \phi > 0.9 \quad (19)$$

Further, a numerical correlation for the interfacial convective heat transfer coefficient was proposed by Kuwahara et al. [31] for a laminar flow as,

$$\frac{h_i D}{k_f} = \left(1 + \frac{4(1-\phi)}{\phi}\right) + \frac{1}{2}(1-\phi)^{1/2} Re_D Pr^{1/3}, \text{ valid for } 0.2 < \phi < 0.9. \quad (20)$$

Results in Eq. (20) depend on the porosity and are valid for packed beds of particle diameter  $D$ . In addition, Saito and de Lemos [22] also obtained the interfacial heat transfer coefficient for laminar flows through an infinite square rod array using the same methodology as Kuwahara et al. [31].

The interstitial heat transfer coefficient  $h_i$  is calculated by correlations Eq. (20) for laminar flow. However, since the relative movement between phases is seen as the promoter of convective heat transport from the fluid to the solid, or vice-versa, a relative Reynolds number defined as,

$$Re_D = \frac{\rho |\mathbf{u}_{rel}| D}{\mu} \quad (21)$$

is used in the correlation Eq. (20) instead of a Reynolds number based on the absolute velocity of the fluid phase. Accordingly, when the solid phase velocity approaches the fluid velocity, the only mechanism for transferring heat between phases is conduction.

## 2. Numerical method and boundary conditions

The problem under investigation is a flow through a channel completely filled with a porous medium, as shown in Fig. 1a. Boundary conditions for laminar flows in porous media are similar to the clear channel flow. The numerical method used to discretize the flow and energy equations was Control Volume approach. The SIMPLE method of Patankar [32] was used to handle the pressure-velocity coupling and applied for relaxing the systems of algebraic equations.

Fig. 1b presents a typical control volume written in the generalized coordinates system  $\eta - \xi$ . The discretized form of the two-dimensional conservation equation for a generic property  $\varphi$ , in permanent regime, is given by:

$$I_e + I_w + I_n + I_s = S_\varphi \quad (22)$$

where  $I_e$ ,  $I_w$ ,  $I_n$  and  $I_s$  represent, respectively, the fluxes of  $\varphi$  in the faces east, west, north and south of the control volume and  $S_\varphi$  its source term.

**Table 2**  
Physical properties of solid and fluid used in Eqs. (28) and (29).

$k_f$ (W/m K)	$\rho_f$ (kg/m <sup>3</sup> )	$c_{pf}$ (J/kg K)	$\mu$ (Ns/m <sup>2</sup> )	$T$ (K)
Fluid: water vapour				
0.0345	0.4345	1986.8	$173.1 \times 10^{-7}$	507.5
Solid: silicon dioxide				
$k_s$ (W/m K)	$\rho_s$ (kg/m <sup>3</sup> )	$c_{ps}$ (J/kg K)	$T$ (K)	
1.38	2220	745	300	

Standard source term linearization is accomplished by using,

$$S_\varphi \approx S_\varphi^{**} \langle \varphi \rangle_p^i + S_\varphi^* \quad (23)$$

Discretization of the momentum equation in the  $x$ -direction gives,

$$S^{*x} = (S_e^{*x})_p - (S_w^{*x})_p + (S_n^{*x})_p - (S_s^{*x})_p + S_p^* \quad (24)$$

$$S^{**x} = S_\varphi^{**} \quad (25)$$

where  $S^{*x}$  is the diffusive part, here treated in an implicit form. The second term,  $S^{**x}$ , entails the additional drag forces due to the porous matrix, which are here treated explicitly.

Convergence was monitored in terms of the normalized residue, which was set to be lower than  $10^{-9}$ .

Boundary conditions are given by:

On the solid walls:

$$\langle \mathbf{u} \rangle^i = 0, \quad q_w = 0 \quad (26)$$

On the entrance:

$$\mathbf{u}_D = \mathbf{u}_{inlet}, \quad \langle T_f \rangle^i = T_{inlet}^f, \quad \langle T_s \rangle^i = T_{inlet}^s \quad (27)$$

## 3. Results and discussion

The problem under investigation is a laminar flow through a channel completely filled with a moving layer of a porous material, as depicted in Fig. 1a. The channel shown in Fig. 1a has length and height given by  $L$  and  $H$ , respectively. As mentioned previously, the geometry of Fig. 1a was numerically investigated using the control-volume method of Fig. 1b. The porous matrix moves with constant velocity  $\mathbf{u}_s$ . Here, validation of the presented simulations considered a fixed solid matrix, i.e.,  $\mathbf{u}_s/\mathbf{u}_D = 0$ , for which an analytical solution is available in the literature [16]. Additional results follow taking into consideration  $\mathbf{u}_s/\mathbf{u}_D > 0$ . All runs for moving bed cases are detailed in Table 3. Also, the fluid and solid phases are given different temperatures at the inlet.

### 3.1. Code validation

Since the problem presented in Nakayama et al. [16] is similar to the problem showed in this work, we used the analytical solution presented by them in order to access the accuracy of the developed code. More specifically, we applied the analysis of Ref. [16] to the case of one-dimensional thermally developing stagnant flow through a semi-infinite porous medium. Although it is recognized that the main objective herein is the analysis a moving bed, the scarcity of experimental data in the literature, which considers a moving fluid through permeable media, limit us to compare our results with those for the stagnant fluid analysis of Ref. [16]. As more data is gathered in the literature, a more in-depth and complete validation procedure can be pursued. For the time being, however, comparisons with analytical solutions for interstitial heat transfer in stagnant fluid are expected to suffice.

Fig. 2 shows values for the longitudinal non-dimensional temperature profiles compared with the analytical solution by Nakayama et al. [16], written as,

**Table 3**  
Cases and parameters used.

Cases investigated	Dimensional				Non-dimensional							
	$u_o$ [m/s]	$u_s$ [m/s]	$u_w$ [m/s]	$K$ [m <sup>2</sup> ]	$Re_D$	$u_s / u_D$	$Da$	$\phi$	$(\rho c_p)_s / (\rho c_p)_f$	$k_s / k_f$		
Effect of $Re_D$	5.666E-02	2.833E-02	2.833E-02	2.025E-05	1.00E01	5.0E-01	3.371E-03	0.9	1.5E00	2.5E01		
	2.833E-01	1.416E-01	1.417E-01		5.00E01							
	5.666E-01	2.833E-01	2.833E-01		1.00E02							
Effect of $u_s / u_D$	2.833E-01	0.000E00	2.833E-01	2.025E-05	1.00E02	0.0E00	3.371E-03	0.9	1.5E00	2.5E01		
		7.083E-02	2.125E-01		7.50E01	2.5E-01						
		1.416E-01	1.417E-01		5.00E01	5.0E-01						
		2.125E-01	7.083E-02		2.50E01	7.5E-01						
		2.692E-01	1.417E-02		5.00E00	9.5E-01						
		5.625E-07	6.25E00		9.365E-05							
Effect of $Da$	2.125E-01	1.062E-01	1.062E-01	5.062E-06	1.87E01	5.0E-01	8.429E-04	0.9	1.5E00	2.5E01		
				5.625E-05	6.25E01		9.365E-03					
				3.086E-07			5.139E-05					
Effect of $\phi$	2.125E-01	1.062E-01	1.062E-01	6.25E01	5.0E-01	5.0E-01	2.601E-04	0.4	1.5E00	2.5E01		
							1.562E-06				1.850E-03	0.6
							1.111E-05					0.8
Effect of $(\rho c_p)_s / (\rho c_p)_f$	2.125E-01	1.062E-01	1.062E-01	9.000E-06	2.50E01	5.0E-01	1.498E-03	0.9	2.5E-01	2.5E01		
									5.0E-01			
									1.0E00			
									1.0E01			
Effect of $k_s / k_f, u_s / u_D = 0$	2.125E-01	0.000E00	2.125E-01	1.562E-06	1.25E02	0.0E00	2.601E-04	0.6	1.5E00	1.0E00		
									1.0E01			
									1.0E02			
									1.0E03			
									1.0E00			
Effect of $k_s / k_f, u_s / u_D = 0.1$	2.125E-01	2.125E-2	1.912E-01	1.562E-06	1.12E02	1.0E-01	2.601E-04	0.6	1.5E00	1.0E01		
									1.0E01			
									1.0E02			
									1.0E03			
									1.0E00			
Effect of $k_s / k_f, u_s / u_D = 0.4$	2.125E-01	8.500E-2	1.275E-01	1.562E-06	7.50E01	4.0E-01	2.601E-04	0.6	1.5E00	1.0E01		
									1.0E01			
									1.0E02			
									1.0E03			
									1.0E00			

$$\theta_f = \frac{\langle T \rangle^f - T_{\min}}{T_{\max} - T_{\min}}$$

$$= 1 + \left\{ \frac{\alpha \frac{k_s}{k_f} \left( 1 - \phi + \left( \frac{k_s}{k_f} - 1 \right) G \right)}{\left[ Pe + \alpha \left( \frac{k_{eff} + K_{xx}}{k_f} \right) \right]} \right\} \times (\exp(-\alpha X) - 1) \tag{28}$$

$$\theta_s = \frac{\langle T \rangle^s - T_{\min}}{T_{\max} - T_{\min}}$$

$$= 1 + \left\{ \frac{\alpha \frac{k_s}{k_f} \left( 1 - \phi + \left( \frac{k_s}{k_f} - 1 \right) G \right)}{\left[ Pe + \alpha \left( \frac{k_{eff} + K_{xx}}{k_f} \right) \right]} \right\} \times (\exp(-\alpha X) - 1) - \exp(-\alpha X) \tag{29}$$

where  $Pe$  is the Peclet number given by

$$Pe = \frac{Pe_d}{(6(1 - \phi)(2 + 1.1Pr_f^{-4/15}Pe_d^{0.6}))^{0.5}} \tag{30}$$

with,

$$Pe_d = \frac{\rho_f c_{pf} |\mathbf{u}_D| D}{k_f} \tag{31}$$

$X$  is a dimensionless coordinate given by:

$$X = \frac{x}{\sqrt{\frac{k_f}{a_i h_i}}} \tag{32}$$

The tortuosity parameter present in Eqs. (28) and (29), is given by:

$$G = \frac{\frac{k_{sg}}{k_f} - \phi - 1(1 - \phi) \frac{k_s}{k_f}}{\left( \frac{k_s}{k_f} - 1 \right)^2} \tag{33}$$

As discussed in Hsu et al. [33], the tortuosity parameter  $G$  is always negative and depends only on the local interfacial geometry and on the solid and fluid thermal properties. According to [33], the tortuosity effect is to reduce the effective thermal conductivity

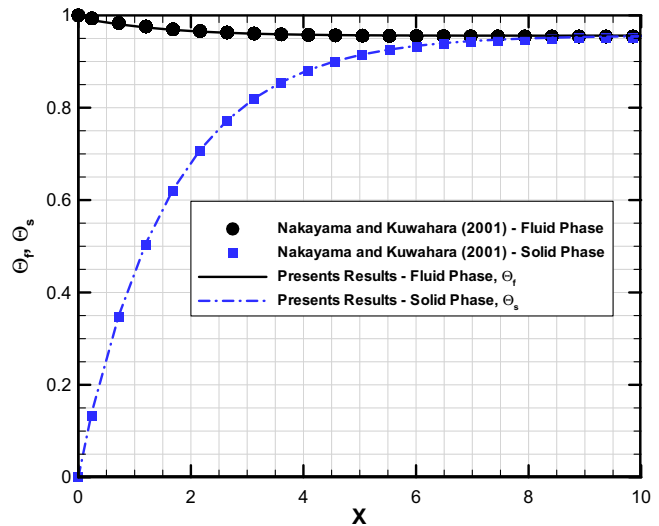


**Fig. 2.** Comparison of dimensionless temperature profiles  $\theta_f$  and  $\theta_s$  with those presented in Nakayama et al. [16].

by increasing the thermal path. In our case, the tortuosity tensor appears only in the one energy equation model, as shown in Rocamora and de Lemos [20]. In this work, what corresponds to the tortuosity parameter  $G$  in Eq. (33) is the model for local conduction shown in Eq. (16).

Further, the tortuosity coefficient and the thermal dispersion, which appear in the model of Nakayama et al. [16], are not considered in our model. Here, we assume that in a one-dimensional problem, the most important and relevant parameter in this case is the film coefficient  $h_i$ , which accounts for the heat exchange between the phases. As mentioned before, an assumption made here is that the overall thermal resistance between the two phases is controlled by the interfacial heat transfer coefficient rather than by the thermal resistance within each phase.

Therefore, for comparisons with the analytical solution presented in Ref. [16], which used for  $h_i$  the expression of Wakao

et al. [30], Eq. (19), we forced the coefficient  $h_i$  in the two approaches to be equal. Or say, we compared Eq. (20) to Eq. (19) when computing the same value of  $h_i$ . By doing this, we found that the values of porosity and particle diameter had to be different in each equation in order to get the same coefficient  $h_i$ . Thus, we found a porosity  $\phi = 0.7$  and a particle diameter  $D = 0.044$  m in our case (Eq. (20)), which gave the same value of  $h_i$  used in Ref. [16] with a different porosity  $\phi = 0.4$ , and particle diameter  $D = 0.04$  m in Eq. (19).

As a result of keeping the same value of  $h_i$ , using distinct porosities in both approaches, we obtained results very close to those by Nakayama et al. [16], as can be seen in Fig. 2, with a relative error of order of  $10^{-3}$ . Further, the effective stagnant thermal conductivity of saturated porous medium  $k_{stg}$  is given by Hsu et al. [33] as,

$$\frac{k_{stg}}{k_f} = 1 - (1 - \phi)^{2/3} + \frac{[(1 - \phi)^{2/3} \frac{k_s}{k_f}]}{[(1 - \phi)^{1/3} \frac{k_s}{k_f} + (1 - \phi)^{1/3}]} \quad (34)$$

The axial component of thermal dispersion tensor  $K_{xx}$  in Wakao and Kagueli [34] is given by,

$$\frac{K_{xx}}{k_f} = 0.5Pe_d \quad (35)$$

In Eqs. (28) and (29)  $-\alpha$  is the negative real root that can be uniquely determined from the cubic characteristic equation that is discussed in detail in Nakayama et al. [16]. The parameters calculated according to the expressions found in [16] are shown in Table 1. The properties of solid and fluid were such that  $k_s/k_f = 40$ . They are presented in Table 2. It is clearly seen from Fig. 2 that good agreement between the numerical solution of Eqs. (11) and (12) and the analytical solution given by Eqs. (28) and (29) was obtained.

The influence of the flow and material properties on the temperature distributions of solid and fluid phases are show next. The simulations to follow were run for concurrent laminar flow and considered the effect of varying the Reynolds number, the phase velocity ratio, permeability, porosity and the ratio of thermal capacity of solid and fluid.

### 3.2. Effect of Reynolds number, $Re_D$

Fig. 3a shows values for the longitudinal non-dimensional temperature profiles as a function of  $Re_D$ . The Reynolds number was calculated based on relative velocity  $\mathbf{u}_{rel}$  and for a slip ratio  $u_s/u_D = 0.5$ . As such, for increasing  $Re_D$  while keeping  $u_s/u_D$  constant, both the fluid and the solid phases had to increase according to the relationship for concurrent flow,

$$Re_D = \frac{\rho \mathbf{u}_{rel} D}{\mu} = \frac{\rho u_D D}{\mu} \left(1 - \frac{u_s}{u_D}\right) = Re \left(1 - \frac{u_s}{u_D}\right) \quad (36)$$

Back to Fig. 3, one can see that the cold fluid is heated up as it permeates the hot porous structure. Also, because the magnitude of both velocities increase for a higher  $Re_D$ , one can see that the axial length needed for reaching the equilibrium value is increased as  $Re_D$  increases.

### 3.3. Effect of slip ratio, $u_s/u_D$

Fig. 3b shows temperature profiles for a moving bed, as a function of  $\mathbf{u}_s/\mathbf{u}_D$ . It is observed that the higher the value of  $\mathbf{u}_s/\mathbf{u}_D$ , the greater is the temperature difference between fluid and solid phases. The stronger axial convection due to a higher  $u_s$  brings more solid phase energy into the reactor, leading to high values of the solid temperature along the axial direction. In addition, increasing  $\mathbf{u}_s/\mathbf{u}_D$  for the same fluid velocity leads to a raise in the equilibrium temperature as more thermal energy is brought into the system. When the solid velocity approaches that of the fluid, the velocity of the solid phase becomes large, leading to a longer equilibrium length. Further, decreasing the relative velocity between phases as  $u_s$  increases reduces the interstitial heat transfer rate and, consequently, exchange of heat between phases becomes mostly governed by conduction, which further contributes towards a longer axial length for thermal equilibrium to be established.

### 3.4. Effect of Darcy number, $Da$

Fig. 4a presents the effect of particle diameter  $D$  on the axial temperature profiles. For a give particle diameter, permeability is given according to the Ergun equation by (see [22]):

$$K = \frac{D^2 \phi^2}{144(1 - \phi)^2} \quad (37)$$

leading to a Darcy number  $Da = K/H^2$  where  $H$  is the height of channel. The Reynolds number and the porosity are kept constant for all curves. It is observed in Fig. 4 that for a small permeability, as a result of a decrease of particle diameter while keeping the porosity constant, a larger interfacial heat transfer area promotes heat

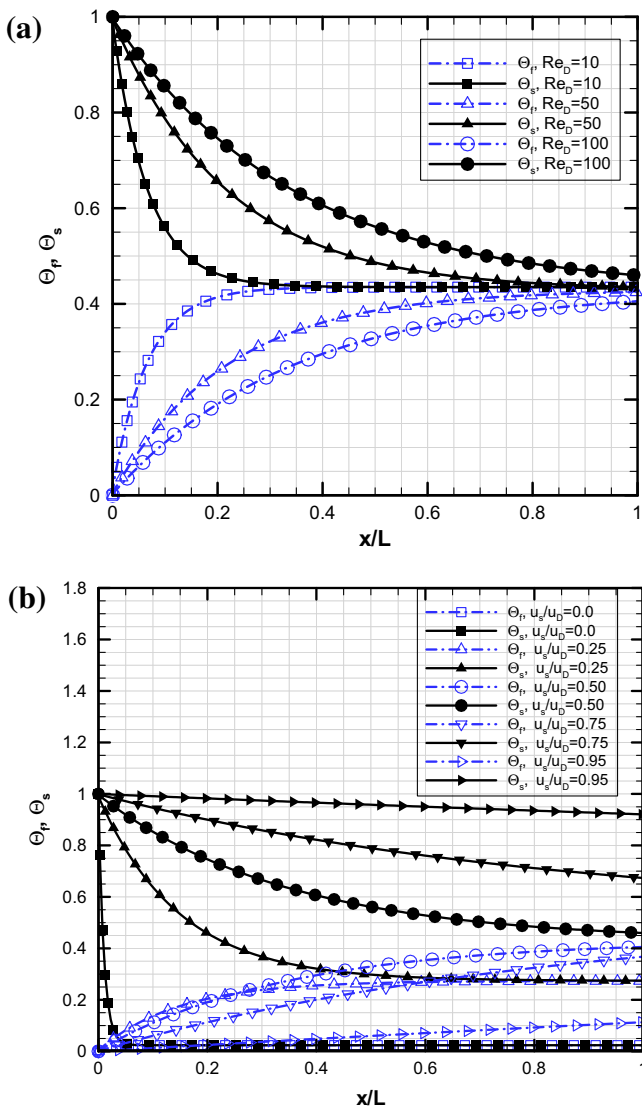


Fig. 3. Non-dimensional temperatures for  $k_s/k_f = 25$ ,  $\phi = 0.9$ ,  $Da = 3.371 \times 10^{-3}$ ,  $(\rho c_p)_s/(\rho c_p)_f = 1.5$ , (a) as a function of  $Re_D$ ,  $u_s/u_D = 0.5$ , (b) as a function of  $u_s/u_D$ .

transfer between phases and reduces the length necessary for thermal equilibrium to be reached.

3.5. Effect of porosity,  $\phi$

Fig. 4b shows the effect of porosity on the longitudinal temperature distribution. The Reynolds number  $Re_D$ , the velocity ratio between the solid and fluid phases  $u_s/u_D = 0.5$  and the ratio of thermal capacity  $(\rho c_p)_s/(\rho c_p)_f = 1.5$  are kept constant for all curves. For a small porosity, a larger interfacial heat transfer area promotes heat transfer between phases and reduces the length necessary for thermal equilibrium to be reached. Also, for a fixed Reynolds number based on  $u_D = \phi \langle u \rangle^i$ , an increase in porosity corresponds to a reduction in the fluid velocity  $\langle u \rangle^i$ , which further reduces the cooling effect by reducing the interfacial heat transfer coefficient  $h_i$  between phases. Consequently, the product  $h_i a_i$  will be decreased as porosity  $\phi$  increases, which indicates damping of convective transfer through the interfacial area.

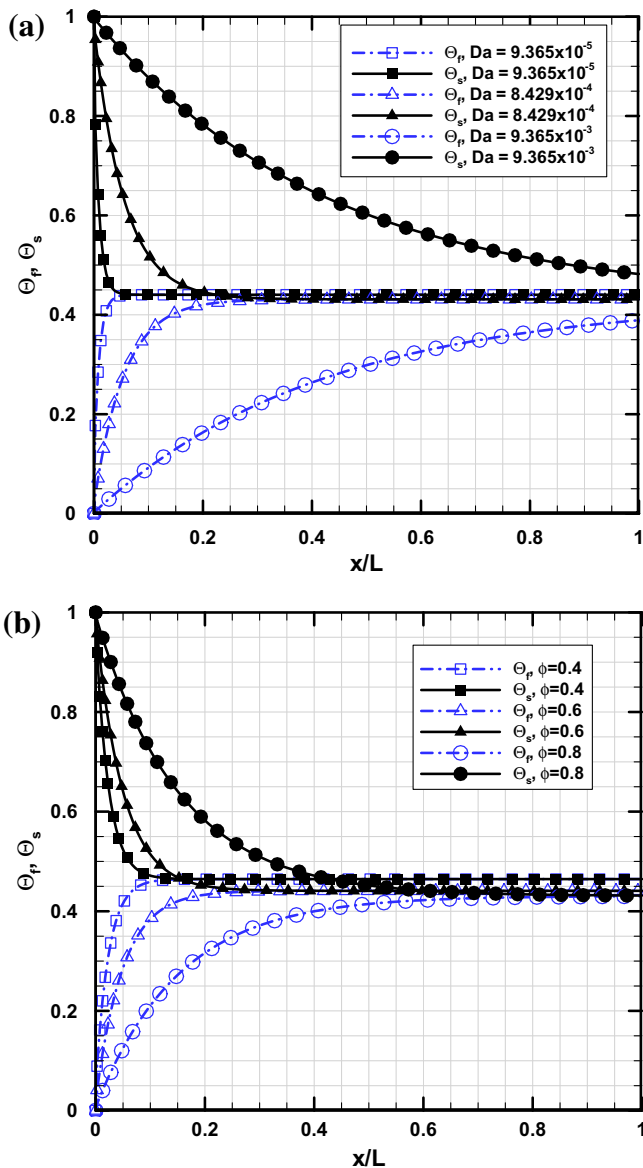


Fig. 4. Non-dimensional temperatures for  $u_s/u_D = 0.5$ ,  $(\rho c_p)_s/(\rho c_p)_f = 1.5$ ,  $k_s/k_f = 25$ ; (a) as a function of  $Da$ ,  $\phi = 0.9$ , (b) as a function of  $\phi$ ,  $Re_D = 62.5$ .

3.6. Effect of thermal capacity ratio  $(\rho c_p)_s/(\rho c_p)_f$

Fig. 5 shows the effect of the thermal capacity ratio on dimensionless temperature distribution along the axial direction. The density and specific heat of the fluid are kept constant given by  $\rho = 0.4345 \text{ kg/m}^3$  and  $(c_p)_f = 1986.8 \text{ J/kg K}$ , respectively. It is observed in Fig. 5 that increasing the thermal capacity of the solid  $(\rho c_p)_s$ , the equilibrium temperature tends to approach the inlet of the solid, or say, for higher values of  $(\rho c_p)_s$  more energy exchange is needed to vary the temperature of the solid by a certain amount.

3.7. Effect of thermal conductivity ratio  $k_s/k_f$

Fig. 6a shows the effect of  $k_s/k_f$  on longitudinal non-dimensional temperatures. It is noted that the higher the ratio  $k_s/k_f$ , the longer is the length needed for thermal development since heat is transported only by conduction within the solid, which causes its temperature distribution to be more connected to the inlet temperature. In addition, a longer developing length and a higher equilibrium temperature are obtained as  $k_s/k_f$  increases.

With increasing  $k_s/k_f$  for  $u_s/u_D = 0.1$  (Fig. 6b), also here we can note higher solid temperatures along the reactor as well higher equilibrium temperatures of the system. Enhancing convection of the solid also raises the equilibrium temperature (see Fig. 3b), which can be better seen when comparing corresponding final equilibrium values for  $k_s/k_f = 1$  in Fig. 6a and b. On the other hand, by decreasing the thermal conductivity ratio, also here a shorter axial length is needed for the equilibrium temperature to be reached.

Further increasing the slip ratio to  $u_s/u_D = 0.4$  (Fig. 6c), one can see that the axial convection strength of the solid for  $k_s/k_f = 1$ , when compared to the similar cases in Figs 6a and b, yield the most significant changes in raising the equilibrium temperature. For example, nondimensional equilibrium temperatures rise from around 0.02 for  $u_s/u_D = 0$  and  $k_s/k_f = 1$  (Fig. 6a) to more than 0.35 for  $u_s/u_D = 0.4$  and the same thermal conductivity ratio equal to unity (Fig. 6a).

Therefore, when comparing the two mechanisms, namely advection and conduction of the solid phase, higher ratios  $k_s/k_f$  have less impact on raising the equilibrium temperature than the increase in the velocity ratio  $u_s/u_D$ .

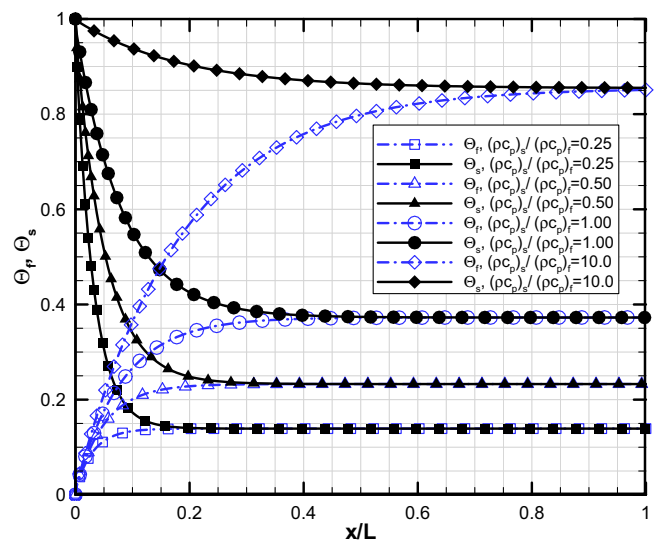


Fig. 5. Non-dimensional temperatures as a function of  $(\rho c_p)_s/(\rho c_p)_f$ ,  $u_s/u_D = 0.5$ ,  $k_s/k_f = 25$ ,  $\phi = 0.9$ ,  $Da = 1.498 \times 10^{-3}$ ,  $Re_D = 25$ .

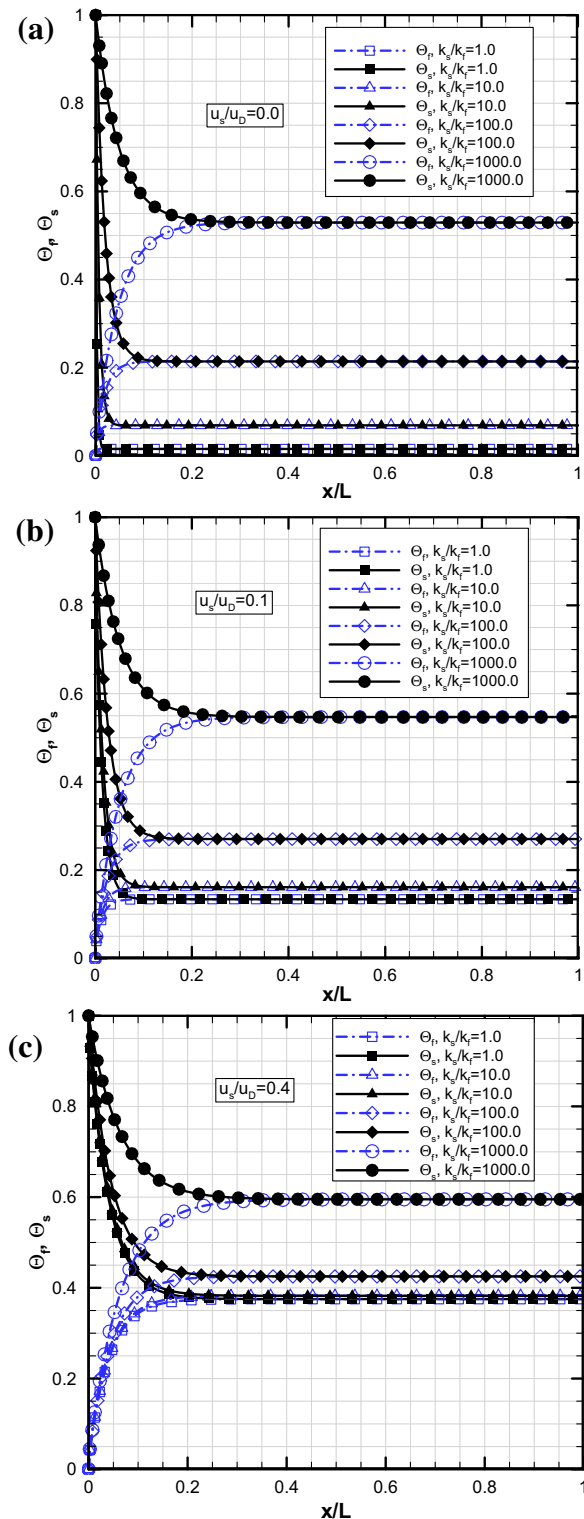


Fig. 6. Non-dimensional temperatures as a function of  $k_s/k_f = 0.6$ ,  $Da = 2.601 \times 10^{-4}$ ,  $(\rho c_p)_s/(\rho c_p)_f = 1.5$ , (a)  $u_s/u_D = 0.0$ , (b)  $u_s/u_D = 0.1$  and (c)  $u_s/u_D = 0.4$ .

#### 4. Conclusions

This paper investigated the behavior of a two-energy equation model to simulate flow and heat transfer in a moving porous bed. Numerical solutions for laminar flow in a moving porous bed were obtained for different Reynolds number  $Re_D$ , slip ratio

$u_s/u_D$ , Darcy number  $Da$ , porosity  $\phi$ , ratio of thermal capacity  $(\rho c_p)_s/(\rho c_p)_f$  and of ratio of thermal conductivity  $k_s/k_f$ , ranging the slip ratio  $u_s/u_D$ . Governing equations were discretized and numerically solved. The following conclusions were observed:

- (1) For a stagnant fluid, excellent agreement was obtained when comparing the results herein with the analytical solution by Nakayama et al. [16], which was used for validating the accuracy of the computational code developed.
- (2) For low values of  $Re_D$ ,  $u_s/u_D$ ,  $Da$ ,  $\phi$ ,  $(\rho c_p)_s/(\rho c_p)_f$  and  $k_s/k_f$ , thermal equilibrium between phases require smaller axial lengths.
- (3) Increasing the speed of the solid relative to a fixed fluid speed enhances the solid convection strength through the reactor as well as reduces the transport of energy between the phases, leading, ultimately, to an increase in the axial length necessary for thermal equilibrium to occur. The results presented here have a wide application to analysis and optimization of engineering processes in which a moving bed configuration could be identified.

#### Acknowledgments

The authors are thankful to CNPq, Brazil, for their financial support during the course of this research.

#### References

- [1] D.R. Parisi, M.A. Laborde, Modeling of counter current moving bed gas-solid reactor used in direct reduction of iron ore, *Chem. Eng. J.* 104 (2004) 35–43.
- [2] E.D. Negri, O.M. Alfano, M.G. Chiovetta, Direct reduction of hematite in a moving-bed reactor: analysis of the water gas shift reaction effects on the reactor behavior, *Am. Chem. Soc.* 30 (1991) 474–482.
- [3] M.S. Valipour, M.Y.M. Hashemi, Y. Saboohi, Mathematical modeling of the reaction in an iron ore pellet using a mixture of hydrogen, water vapor, carbon monoxide and carbon dioxide: an isothermal study, *Adv. Powder Technol.* 17 (3) (2006) 277–295.
- [4] M.S. Valipour, Y. Saboohi, Modeling of multiple noncatalytic gas–solid reactions in a moving bed of porous pellets based on finite volume method, *Heat Mass Transfer* 43 (9) (2007) 881–894.
- [5] M.S. Valipour, Y. Saboohi, Numerical investigation of nonisothermal reduction hematite using syngas: the shaft scale study, *Modeling Simul. Mater. Sci. Eng.* 15 (2007) 487–507.
- [6] R. Henda, D.J. Falcioni, Modeling of heat transfer in a moving packed bed: case of the preheater in nickel carbonyl process, *J. Appl. Mechanics – ASME* 73 (1) (2006) 47–53.
- [7] C. Ryu, Y.B. Yang, A. Khor, N.E. Yates, V.N. Sharifi, J. Swithenbank, Effect of fuel properties on biomass combustion: part I. Experiments–fuel type, equivalence ratio and particle size, *Fuel* 85 (2006) 1039–1046.
- [8] C. Boman, A. Nordin, L. Thaning, Effects of increased biomass pellet combustion on ambient air quality in residential areas – a parametric dispersion modeling study, *Biomass and Bioenergy* 24 (2003) 465–474.
- [9] T. Shimizu, J. Han, S. Choi, L. Kim, H. Kim, Fluidized-bed combustion characteristics of cedar pellets by using an alternative bed material, *Energy Fuels* 20 (2006) 2737–2742.
- [10] T.K. Kayal, M. Chakravarty, Mathematical modeling of continuous updraft gasification of bundled jute stick – a low ash content woody biomass, *Bioresour. Technol.* 49 (1) (1994) 61–73.
- [11] A. Rogel, J. Aguilón, The 2D Eulerian approach of entrained flow and temperature in a biomass stratified downdraft gasifier, *Am. J. Appl. Sci.* 3 (10) (2006) 2068–2075.
- [12] T. Nussbaumer, Combustion co-combustion of biomass: fundamentals technologies and primary measures for emission reduction, *Energy Fuels* 17 (2003) 1510–1521.
- [13] S.Y. Li, R.S. Bie, Modeling the reaction of gaseous HCl with CaO in fluidized bed, *Chem. Eng. Sci.* 61 (16) (2006) 5468–5475.
- [14] J. Zhao, J. Huang, J. Wu, Y. Fang, Y. Wang, Modeling and optimization of the moving granular packed bed for combined hot gas desulfurization and dust removal, *Powder Technol.* 180 (2008) 2–8.
- [15] J. Baron, E.M. Bulewicz, The combustion of polymer pellets in a bubbling fluidized bed, *Fuel* 85 (2006) 2494–2508.
- [16] A. Nakayama, F. Kuwahara, M. Sugiyama, G. Xu, A two energy equation model for conduction convection in porous media, *Int. J. Heat Mass Transfer* 44 (2001) 4375–4379.
- [17] M. Quintard, Modeling local non-equilibrium heat transfer in porous media, *Proc. Eleventh Int. Heat Transfer Conf.* 1 (1998) 279–285.

- [18] M. Kaviany, *Principles of Heat Transfer in Porous Media*, 2nd ed., Springer, New York, 1995. pp. 391–424.
- [19] C.T. Hsu, A closure model for transient heat conduction in porous media, *J. Heat Transfer* 121 (1999) 733–739.
- [20] F.D. Rocamora Jr., M.J.S. de Lemos, Analysis of convective heat transfer of turbulent flow in saturated porous media, *Int. Comm. Heat and Mass Transfer* 27 (6) (2000) 825–834.
- [21] E.J. Braga, M.J.S. de Lemos, Laminar natural convection in cavities filled with circular and square rods, *Int. Commun. Heat Mass Transfer* 32 (10) (2005) 1289–1297.
- [22] M.B. Saito, M.J.S. de Lemos, Interfacial heat transfer coefficient for non-equilibrium convective transport in porous media, *Int. Comm. Heat and Mass Transfer* 32 (5) (2005) 666–676.
- [23] M.B. Saito, M.J.S. de Lemos, A correlation for interfacial heat transfer coefficient for turbulent flow over an array of square rods, *J. Heat Transfer* 128 (2006) 444–452.
- [24] M.B. Saito, M.J.S. de Lemos, Laminar heat transfer in a porous channel simulated with a two-energy equation model, *Int. Commun. Heat Mass Transfer* 36 (2009) 1002–1007.
- [25] M.J.S. de Lemos, M.B. Saito, Computation of turbulent heat transfer in a moving porous bed using a macroscopic two-energy equation model, *Int. Commun. Heat Mass Transfer* 35 (2008) 1262–1266.
- [26] M.B. Saito, M.J.S. de Lemos, A macroscopic two-energy equation model for turbulent flow and heat transfer in highly porous media, *Int. J. Heat Mass Transfer* 53 (2010) 2424–2433.
- [27] M.J.S. de Lemos, *Turbulence in Porous Media: Modeling and Applications*, Elsevier, Amsterdam, 2006.
- [28] W.G. Gray, P.C.Y. Lee, On the theorems for local volume averaging of multiphase system, *Int. J. Multiphase Flow* 3 (1977) 333–340.
- [29] S. Whitaker, Advances in theory of fluid motion in porous media, *Ind. Eng. Chem.* 61 (1969) 14–28.
- [30] N. Wakao, S. Kagueli, T. Funazkri, Effect of fluid dispersion coefficients on particle–fluid heat transfer coefficient in packed bed, *Chem. Eng. Sci.* 34 (1979) 325–336.
- [31] F. Kuwahara, M. Shirota, A. Nakayama, A numerical study of interfacial convective heat transfer coefficient in two-energy equation model for convection in porous media, *Int. J. Heat Mass Transfer* 44 (2001) 1153–1159.
- [32] S.V. Patankar, *Numerical Heat Transfer and Fluid Flow*, Hemisphere, Washington, DC, 1980.
- [33] C.T. Hsu, P. Cheng, K.W. Wong, A lumped parameter model for stagnant thermal conductivity of porous media, *J. Heat Transfer* 117 (1995) 264–269.
- [34] N. Wakao, S. Kagueli, in: *Heat and Mass Transfer in Packed Beds*, Gordon and Breach, New York, 1982. pp. 243–295.